*International Journal of Engineering and Applied Sciences (IJEAS)*
*Vol.2, Issue 1(2010)44-53*

# GSM/DCS MICROSTRIP ANTENNA DESIGN USING FINITE ELEMENT METHOD

***S. Cumhur BAŞARAN***
*Akdeniz University, The Vocational School of Technical Sciences*
*07058 Antalya, Turkey*

Accepted Date: 10 September 2009

**Abstract**

*A Dual-band microstrip antenna based on split-ring elements is introduced for GSM/DCS (900/1800MHz) applications. The proposed split-ring antenna (SRA) has novel design and provides 2.3% and 3.8% impedance bandwidth performance at the respective bands without a need for additional matching networks. Also, the antenna exhibits uniform radiation patterns at each frequency band. Analysis and design of the proposed microstrip antenna are carried out by means of full-wave simulators based on the finite-element method, namely the in-house Finite Element Microstrip Antenna Simulator (FEMAS) and the commercially available High Frequency Structure Simulator (HFSS). Return-loss characteristics of the antenna using the simulators are in good agreement.*

**Keywords:** *Dual-band; finite element method; GSM, microstrip antenna; Split-ring*

## 1. Introduction

In recent years, mobile communication systems have experienced enormously high marked demand. In the most country, the two operation frequency systems, global system for mobile communication (GSM) operated at 900 MHz and the digital communication system (DCS) at 1800 MHz, are simultaneously used in current mobile communications. Thus, dual-band operation in 900/1800 MHz bands for GSM/DCS are desired to meet the corresponding IEEE standards, preferably using only one antenna element. In these applications, microstrip antennas are highly utilized due to their compact, planar, lightweight, and low-cost features [1-6].

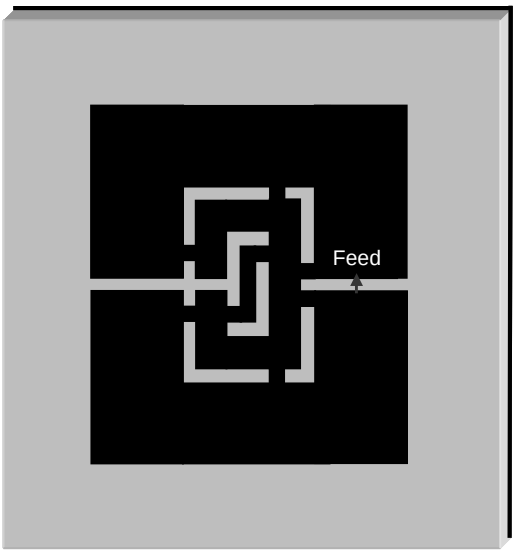


Fig. 1. Proposed GSM/DCS-SRA (top views are shown)

In this paper, i propose a novel GSM/DCS antenna design based on printed split-ring elements. These elements with inherent μ-negative behavior have recently been used as building blocks of various metamaterial structures [7], and they were utilized in various filter applications [8-10]. Moreover, recently a loaded split-ring element has been considered in dual-band wireless local area network (WLAN) antenna configurations [11,12]. The proposed split-ring antenna (SRA) with novel configuration consists of split-ring elements and metallic loadings appropriately placed between the rings as shown in Fig. 1. The antenna is fed by a current-probe placed in one of the splits in its outer ring. The probe basically represents practical coaxial feeding [13], and in the proposed configuration, there is no additional matching network. The compact SRA design provides dual-band operation for GSM/DCS applications.

The analysis and design of SRA has been carried out using two full-wave simulators based on the finite element method, namely the in house FEMAS and the commercially available Ansoft HFSS v.10.0. FEMAS developed myself is not intended to compete with commercial finite element modeling codes. It does not have a sophisticated mesh generator, graphical output, or unlimited technical support. Its primary strengths is ease-of-use, modest resource requirements, and accurate modeling of three-dimensional rectangular patch antenna configurations over a wide range of frequencies. In addition, it is possible to obtain input impedance and return-loss charecterics and also radiation and gain performances of a patch antenna. In the paper, after reviewing the FEM formulation and introducing FEMAS briefly, i present simulation results using the two simulators for the proposed design.

## 2. Analysis Method

The FEM is a well-known frequency-domain technique which is highly capable of modeling 3D complex structures with inhomogeneities [14,15]. In FEM analysis, the structure at hand is first meshed into prism or tetrahedron elements, where unknowns of the problem are usually electric field vector components specified along edges of the elements. The discretized FEM functional is then minimized for each unknown to generate the system matrix, which is mainly sparse. Finally, the FEM system is solved for the edge unknowns via a direct or an iterative solver [14,15].

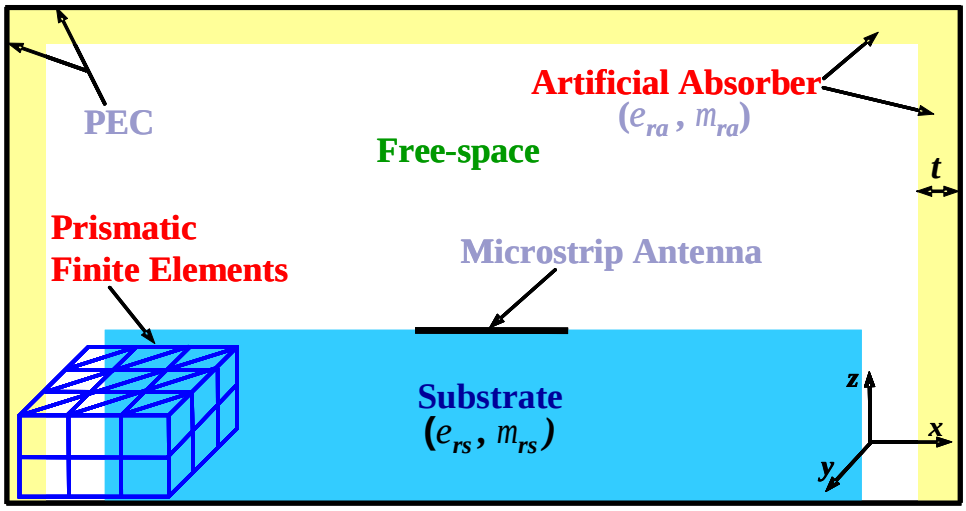


Fig. 2. FEM computational domain for a typical microstrip antenna problem (a cross-section view is shown)

In particular, for open (radiation or scattering) problems the computational domain is truncated by an absorbing boundary condition, an artificial absorber or a perfectly-matched layer to simulate the free-space. Alternatively, rather complicated but more accurate truncation can be realized by hybridizing the FEM with the moment method [14,15].
In this research, i have developed a FEM-based simulator, namely the FEMAS. This analysis tool allows 3D modeling of microstrip antennas using uniform prismatic mesh elements and outcomes the corresponding input impedance, return-loos and radiation pattern characteristics. In particular, the FEMAS has capability of modeling metallic patches, ideal current-probe feeds, shorting pins, resistive cards, impedance loads (in *x*, *y* or *z* directions) within a metal-backed multilayer dielectric substrate. A cross-section view of the 3D computational domain for a typical microstrip antenna problem is depicted in Fig. 2 as an example for FEM modeling employed in the FEMAS. As shown, a microstrip antenna placed over a PEC-backed dielectric substrate with ($\varepsilon_{rs}$, $\mu_{rs}$) radiates to the vacuum-filled upper half-space which is truncated by a PEC-backed artificial absorber with $\varepsilon_{ra}=\mu_{ra}=1-j2.7$ and thickness $t=0.15\lambda_0$ [16]. For converged field analysis, as the distance (in all directions) between the antenna and the artificial absorber is considered to be minimum value $0.25\lambda_0$, each dimension of prismatic finite elements has to be typically smaller than $0.05\lambda_0$.
The FEM formulation in FEMAS starts with the three-dimensional wave equation

$$\nabla\times\left(\frac{1}{m_r}\nabla\times\mathbf{E}\right)-k_0^2 e_r\mathbf{E}=-jk_0Z_0\mathbf{J} \qquad (1)$$

in which **E** represents the total electric field, ($\varepsilon_r$, $\mu_r$) denote the relative permittivity and permeability of the computational domain, $k_0$ is the free space wavenumber and $Z_0$ is the free space intrinsic impedance. In addition, **J** denotes the impressed electric source. With boundary conditions given by

$$\hat{n}\times\mathbf{E}=0 \qquad (2)$$

After multiplying equation (1) by a weighting function w and integrating over the finite element volume V, one obtains the FEM weak form as follows:

$$\int_V\left[\frac{1}{m_r}(\nabla\times\mathbf{E})\cdot(\nabla\times\mathbf{W})-k_0^2 e_r\mathbf{E}\cdot\mathbf{W}\right]dV=-jk_0Z_0\int_V\mathbf{J}\cdot\mathbf{W}\,dV \qquad (3)$$

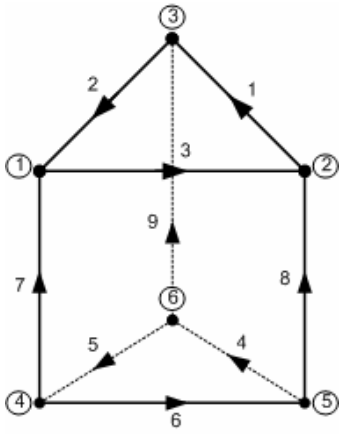

Fig. 3. Right prism finite element

Right prism element shown in Fig. 3 is used to discretize the volume *V*. Basis functions are defined within a prism and are associated with one of the nine edges. The edge basis functions for top triangle edges are given by

$$\mathbf{N}_{ij}^{e} = b_{ij}(L_i^e \nabla L_j^e - L_j^e \nabla L_i^e)s, \qquad i, j = 1,\ 2,\ 3\ \ ;\ \ k = 1,\ 2,\ 3 \tag{4}$$

and those for the bottom edges are

$$\mathbf{N}_{ij}^{e} = b_{ij}(L_i^e \nabla L_j^e - L_j^e \nabla L_i^e)(1-s), \qquad i, j = 1,\ 2,\ 3\ \ ;\ \ k = 1,\ 2,\ 3 \tag{5}$$

and the vertical edges are

$$\mathbf{N}_{k}^{e} = \hat{v}_i(x,h)L_i^e(x,h), \qquad i = 1,\ 2,\ 3\ ; \qquad k = 7,\ 8,\ 9 \tag{6}$$

In the above equations, $L_i^e$ are the node-based shape function and *s* is normalized parameter which is zero at the bottom face and unity at the top face of prism. For the vertical edges, the vector $\hat{v}$ is a linear weighting of the unit vectors $\hat{v}_1$, $\hat{v}_2$, $\hat{v}_3$ associated with the vertical arms and is defined as:

$$\begin{aligned} v(x,h) &= \sum_{i=1}^{3} L_i^e(x,h)\hat{v}_i \\ \hat{v}(x,h) &= \frac{v(x,h)}{|v(x,h)|} \end{aligned} \tag{7}$$

For the calculation of the terms in the above equations (4-7), refer to appendices in [12]. The electric field **E** within volume *V* can be expanded as:

$$\mathbf{E} = \sum_{i=1}^{9} E_i \mathbf{W}_i \tag{8}$$

where $\{E_n\}$ is a set of unknown complex scalar coefficients.

Using the Galerkin approach (setting the weighting functions **W** equal to the basis functions **N**), a discrete form of equation (3) is obtained for each prism:

$$[A_{nm}]\ [E_m] = [B_m] \tag{9}$$

where

$$\begin{aligned} A_{mn} &= \int_V \left[ \frac{1}{m_r}(\nabla \times \mathbf{W}_n)\cdot(\nabla \times \mathbf{W}_m) - jk_0 Z_0 e_r \mathbf{W}_n \cdot \mathbf{W}_m \right] \mathbf{dV} \\ B_m &= \int_V \mathbf{J}\cdot\mathbf{W}_m \mathbf{dS} \end{aligned} \tag{10}$$

The above equation can be obtained for all the prism in the volume of interest. All these individual equations are then combined into a linear global equation system in matrix form.

$$[A]\ [E]=[B] \tag{11}$$

Where [$B$] is a column matrix and is determined on the basis of the boundary conditions or the forced excitation. The matrix [$A$] is square of size $N\times N$ very sparse and typically symmetric. [$E$] is a column matrix and has unknown coefficients defining electrical field values in finite element edge. The related matrix system is solved iteratively by the most affective method which is the complex biconjugate gradient [17].
In this study, I have mainly used the commercial available Ansoft HFSS v.10.0 during the design process, particularly due to its speed advantage. The HFSS is also a FEM-based full-wave analysis tool with dissimilar modeling capabilities as compared to the FEMAS. In particular, the HFSS offers non-uniform meshing while uniform gridding is applicable in the FEMAS. In addition, the truncation schemes differ in each simulator. As a result, slight discrepancies in the HFSS and FEMAS simulation results are observed.

## 3. Antenna Design

In this section, the design steps of proposed SRA are presented and the optimum antenna performance is evaluated. A series of parametric studies was carried out to achieve desired antenna performance, particularly tuning the resonant frequencies and return loss characteristics. In this process, the optimized critical antenna parameters were the substrate's thickness and permittivity, dimensions of the ring elements as well as positions of the metallic loadings.

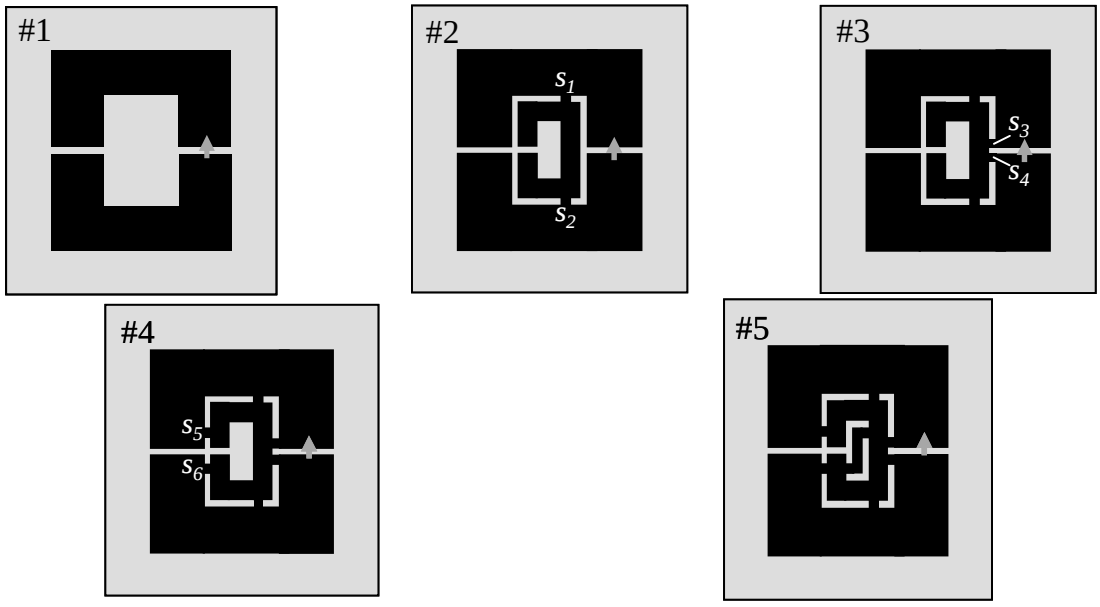


Fig. 4. Design steps for the GSM/DCS antenna

We consider the design steps of the GSM/DCS antenna as displayed in Fig.4. The starting configuration (#1) included only one ring element with two splits. While one of the splits was used for the feed placement, the other one was needed to achieve dual-band performance with the inclusion of a secondary split-ring as well as metallic loadings $s_1$ and $s_2$ inserted between

the rings (#2). The highly resonant impedance characteristics for the configurations #1 and #2 are shown in Fig. 5. As seen, the inner ring with the loadings $s_1$ and $s_2$ provided dual-band profile around 0.6 and 1.3 GHz bands with the impedance levels of 2000 Ohms. In order to decrease those high impedance levels, a secondary set of loadings, namely $s_3$ and $s_4$, was placed between the rings nearby the feeding gap (#3). As shown in Fig. 6, the configuration #3 not only resulted in reduced impedance levels (on the order of several tens Ohms), but also shifted the dual frequency bands to 0.7 and 1.6 GHz. For further frequency adjustment, an additional set of loadings ($s_5$ and $s_6$) was inserted across the rings close to their neighboring splits (#4), thus shifting the respective bands to 0.8 and 1.7 GHz while almost preserving the impedance levels as can be seen in Fig. 6. Finally, an S-shaped loading placed within the inner ring (#5) allowed for the desired dual-band performance at the designated GSM/DCS bands, 900/1800 MHz (Fig. 6.)

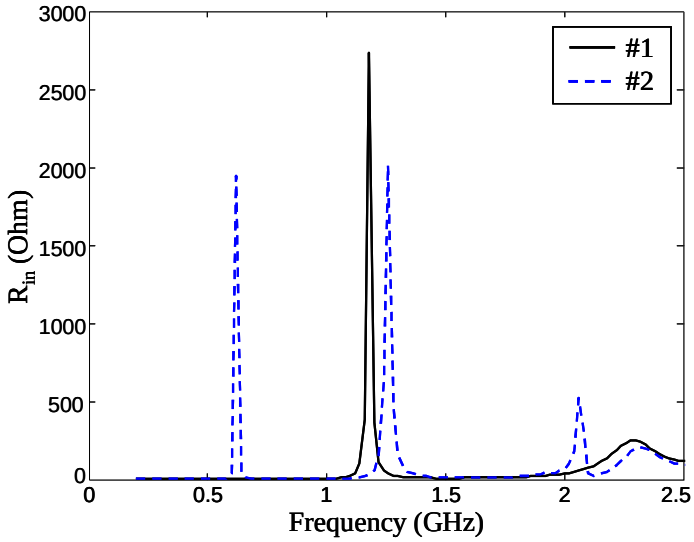


Fig. 5. Real parts ($R_{in}$) of the input impedances for the GSM/DCS antenna design configurations #1 and #2

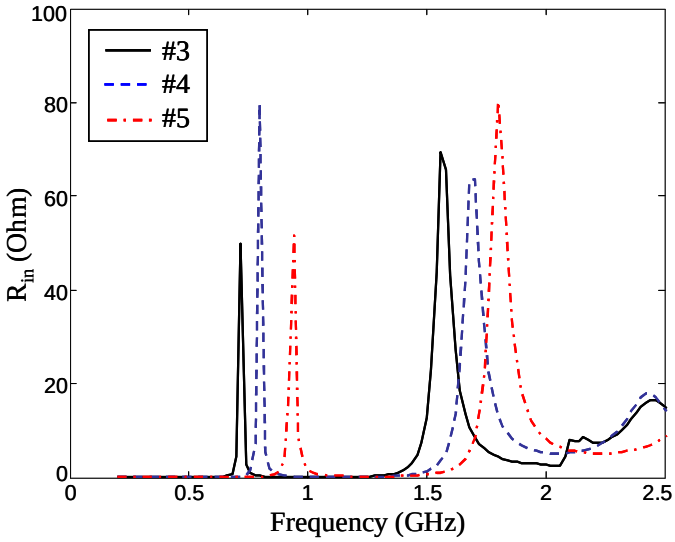


Fig. 6. Real parts ($R_{in}$) of the input impedances for the GSM/DCS antenna design configurations #3, #4 and #5

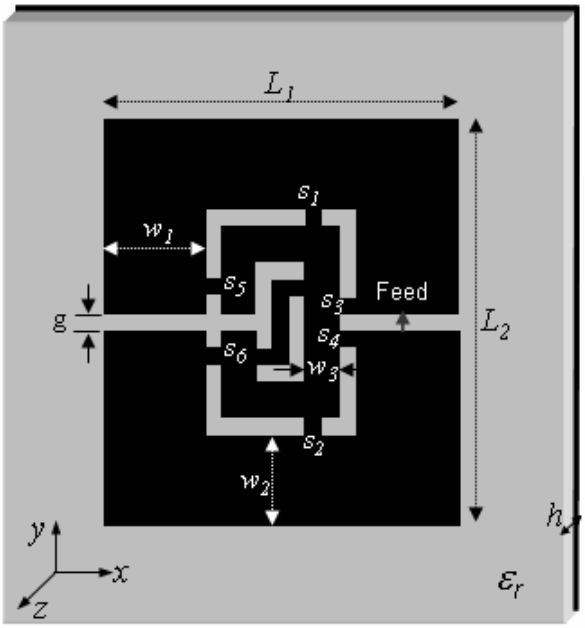


Fig. 7. Proposed SRA design: $s_1$-$s_6$ (metallic loads: 2×2), $L_1$=42, $L_2$=46, $w_1$=12, $w_2$=10, $w_3$=4, $g$=2, $h$=5.08 (all in mm), $e_r$=4.5

The GSM antenna configuration #5 is re-displayed in Fig. 7 with its optimized design parameters. As seen, the SRA composed of two metallic split-rings covers an area of 42×46 mm$^2$ and placed on a grounded Rogers TMM4 substrate with 5.08 mm thickness and dielectric constant of 4.5. The outer ring with two splits is three-times wider than the inner ring with one split only. In addition, each metallic loading inserted appropriately between the ring elements has a size of 2×2 mm$^2$.

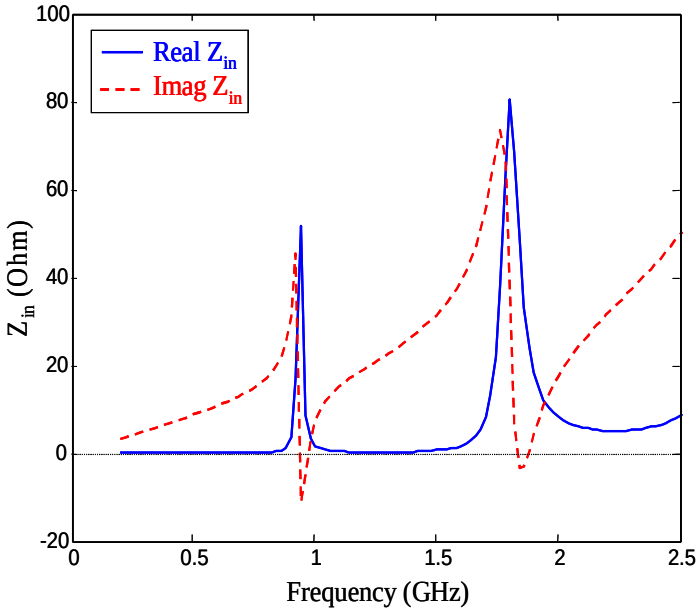


Fig. 8. Input impedance ($Z_{in}$) characteristics of the SRA design

The input impedance and return loss characteristics of the SRA design are displayed in Figs. 8 and 9, respectively. As shown, a dual-band operation is achieved at 940 MHz and 1835 MHz with 2.3% and 3.8% bandwidths, respectively, where $|S_{11}| < -10$dB criterion with 50Ω

system impedance is considered. Note that in Fig. 9 the return loss characteristics are displayed for both simulators used in this study, namely the FEMAS and the HFSS. As seen, the simulation results agree with each other quite well with slight frequency shifts, which are mainly due to different truncation as well as different meshing schemes employed in each simulator.

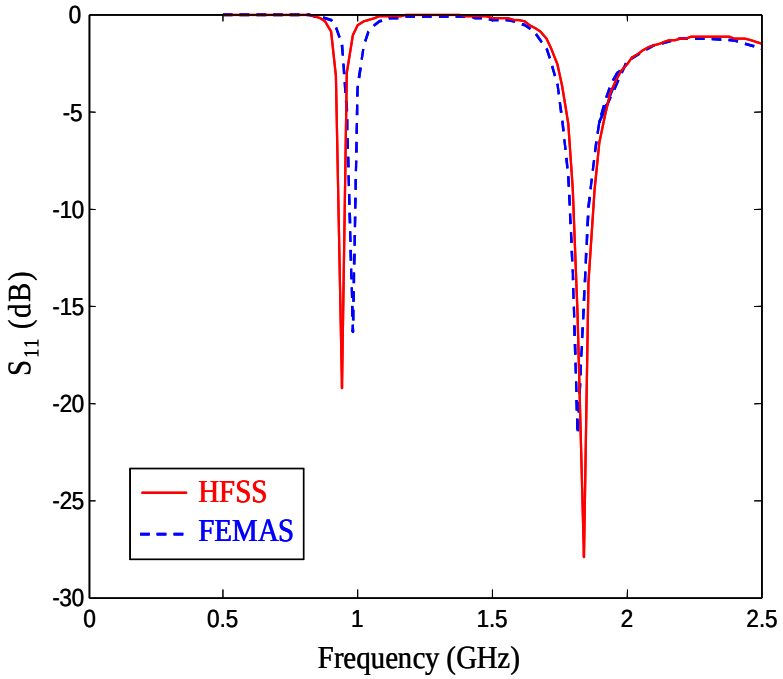


Fig. 9. Return loss ($S_{11}$) characteristics of the SRA design

In addition, radiation patterns of the SRA for the respective frequencies are shown in Fig. 10. As seen, E-plane patterns demonstrate omni-directional characteristics at each operational frequency as desired in GSM/DCS applications. Nevertheless, H-plane patterns show relatively directional behavior.

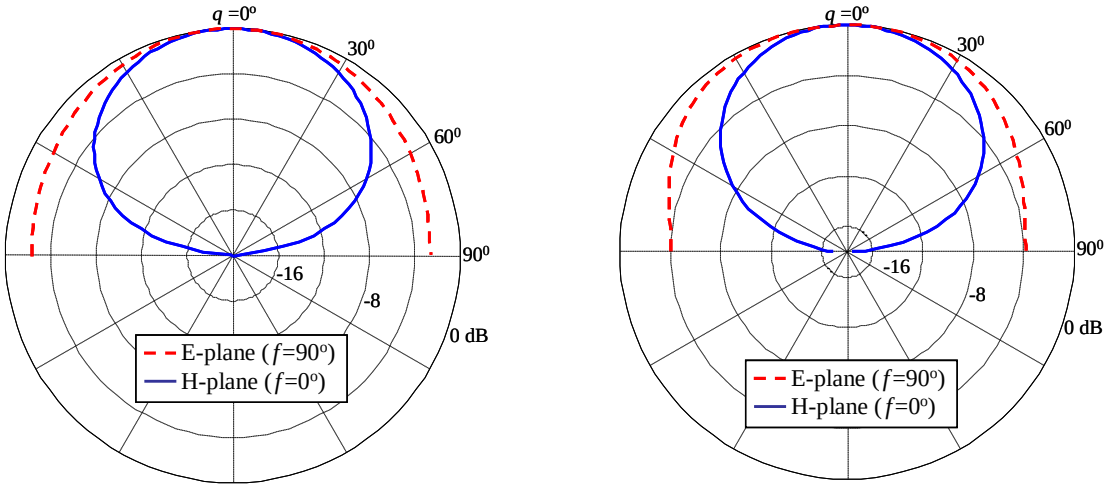


(a) $f$=940 MHz (b) $f$=1835 MHz

Fig. 10. Radiation patterns of the SRA design

## 4. Conclusions

In the paper, a novel GSM antenna based on microstrip split-ring elements with metallic loadings has been proposed. In house microstrip antenna simulator based on finite element method and named as FEMAS has been introduced. I have presented simulated antenna performances obtained by the well-known HFSS and FEMAS. Also, simulated data of the proposed antenna using the simulators are in good agreement. In the antenna design, as the outer-most ring is fed by a current-probe, the inner rings with loadings provide frequency-tuning and impedance matching. Thus, SRA design performs dual-band operation at the respective frequency bands of 900/1800 MHz with 2.3% and 3.8% impedance bandwidths, respectively. Although the corresponding bands may seem rather narrow, note that this performance is achieved without additional matching network, with which broader bandwidth performance is expected.

## References


[1] Yang, M., Chen, Y., A Novel U-Shaped planar microstrip antenna for dual-frequency mobile telephone communications, *IEEE Trans. Antennas Propag.*, 49, 6, 1002-1004, 2001.

[2] Chen, H.-M., Chen, J.-M., Cheng, P.-S., Lin, T.-F., Feed for dual-band printed dipole antenna, *Electron. Lett.*, 40, 21,1320-1322, 2004.

[3] Wong, K.-L., Lin, Y.-C. and Tseng, T.-C., Thin internal GSM/DCS patch antenna for a portable mobile terminal, *IEEE Trans. Antennas Propag.*,, 54, 1, 238-242, 2006.

[4] Lin, C.-I., Wong, K.-L., Printed monopole slot antenna for internal multiband mobile phone antenna, *IEEE Trans. Antennas Propag.*, 55, 12, 3690-3697, 2007.

[5] An, J., Wang, G.-M., Zhang, C.-X. and Zeng, H.-Y., Compact circularly polarized omnidirectional microstrip antenna, *Microwave Opt. Technol. Lett.*, 51, 11, 2643-2646, 2009.

[6] Wu, G.-L., Mu, W., Zhao, G. and Jiao, Y.-C., A novel design of dual circularly polarized antenna feed by L-strip, *Progress In Electromagnetics Research,* PIER 79, 39-46, 2008.

[7] Pendry, J. B., Holden, A. J., Robins, D. J. and Stewart, W. J., Magnetism from conductors and enhanced nonlinear phenomena, *IEEE Trans. Microwave Theory Tech.,* 47, 11, 2075-2084, 1999.

[8] Erdemli Y. E. and Sondas, A., Dual-polarized frequency-tunable composite left-handed slab, *J. Electromagn. Waves and App*., 19, 14, 1907-1918, 2005.

[9] Cenk, C., Sondas, A. and Erdemli, Y. E., Tunable split ring resonator microstrip filter design, in Proc. Mediterranean Microwave Symposium, Genoa, Italy, September 19-21 2006.

[10] Ucar, M. H. B., Sondas, A. and Erdemli, Y. E., Switchable split-ring frequency selective surfaces, *PIERB*, 6, 65-79, 2008.

[11] Basaran S. C. and Erdemli, Y. E., Dual-band split-ring antenna design for WLAN applications, *Turkish J. Elec. Engin. Comp. Sci*., 16, 1, 79-86, 2008.

[12] Basaran S. C. and Erdemli, Y. E., A dual-band split-ring monopole antenna for WLAN applications, *Microwave Opt. Technol. Lett.*, 51, 11, 2685-2688, 2009.

[13] Chen, A.-C., Tang, C.-L. and Lu, H., A Loop antenna for WLAN application, IEEE Asia-Pacific Conference Proceedings, Dec. 4-7, 2005.

[14] Volakis, J. L., Chatterjee, A. and Kempel, L. C., *Finite Element Method for Electromagnetics,* IEEE Press & Oxford University Press; New York, 1998.

[15] Jianming, J., *The Finite Element Method in Electromagnetics,* John Wiley & Sons Inc; New York, 1993.

[16] Ozdemir, T. and Volakis, J. L., A comparative sturdy of an absorber boundary condition and an artificial absorber for truncating finite element mesh, *Radio Sci.,* 29, 255-1263, 1994.
[17] Jacobs, D. A. H., A generalization of the conjugate gradient method to solve complex systems, *IMA J. Numerical Anal.,* 6, 447-452,1986.